A Simple Ultra-Wideband Wake-up Scheme for Semi-Active Sensor Nodes

Florian Troesch and Armin Wittneben
Communication Technology Laboratory, ETH Zurich, CH-8092 Zurich, Switzerland
Email: {troeschf,wittneben}@nari.ee.ethz.ch

***Abstract*— *Ultra-wideband impulse radio* (UWB-IR) merges low complexity system design with good localization capabilities enabling *low-data-rate/location-tracking* (LDR/LT) sensor network design. However power consumption of the sensor nodes is a fundamental problem. Therefore, a simple wake-up scheme for asymmetric network topologies is investigated, where a *static wireless backbone* communicates with many *semi-active* sensor nodes. At sensor side only a low power wake-up detector is active during idle times to reduce power consumption. The wireless backbone consists of distributed UWB-IR devices and triggers the sensor nodes by means of beamforming, exploiting the large UWB-IR bandwidth to highly concentrate energy in a specified area. Conditions for basic feasibility of the scheme are derived and promising performance results based on realistic simulations are presented.**

I. Introduction

Expected localization capabilities combined with the possibility to design low complexity devices make *ultra-wideband impulse radio* (UWB-IR) a promising technology to enhance *low-data-rate* (LDR) sensor networks with localization and tracking functionalities (LDR/TR) [1]. A typical network topology consists of a data source or sink, such as a wireless backbone, which communicates with a sensor field containing a large, varying number of sensor nodes that are densely deployed in an area of interest. While hardware constraints on the backbone can be rather loose, constraints on sensor nodes are stringent. Their production costs should be small and often, they are equipped with very limited power supply. Hence, only simple hardware structures are suited for sensor nodes, minimizing cost, complexity, and power consumption.

Wake-up radio is a known communication scheme proposed for classic ad-hoc networks, to reduce energy consumption during idle times. As power consumption is a fundamental problem in sensor networks, we proposed a similar approach for UWB-IR in [2] adapted to the specific characteristics of UWB-IR. The considered network consists of a large number of *semi-active* sensor nodes and a *static wireless backbone.* During idle times, the semi-active sensor nodes fall into stand-by mode, and only a low power wake-up detector stays active. They have neither position nor channel state information. The wake-up detector is a simple square law detector, which triggers active mode, if it measures an amount of energy corresponding to a wake-up pulse. The wireless backbone consists of cooperating devices, statically mounted on the environment. They are connected wirelessly or by wire to exchange global channel and positioning information and are assumed perfectly synchronized. By beamforming, the backbone system spatially concentrates its radiated energy at a specific location and thus triggers the sensor node at this location to enter active mode. Hence, the backbone centralizes *medium-access-control* (MAC) responsibility of the sensor field.

Based on a simplified signal model and approximations of the probabilities of false alarm and missed detection, basic feasibility of proposed wake-up scheme was shown in [2]. In this work, these approximations are confirmed by exact analysis and performance results based on simulations over measured UWB-IR *channel impulse responses* (CIR). It is demonstrated that presented scheme works well under strong multi-path condition and sampling jitter.

In the following section, the detailed scenario and the signal model are introduced. In Section III, analysis of the proposed scheme is presented, followed by simulation results in Section IV. Finally, Section V provides some conclusions.

II. Signal Model

A. Scenario

The backbone devices are statically mounted on the wall of a circular room with equal spacing d, while the sensor nodes are distributed over the area enclosed by the devices, as shown in Fig. 1. No important scatterers or shadowing objects are present and therefore, *line-of-sight* (LOS) conditions dominate. This scenario is chosen for convenience, as it allows good understanding of the scheme, while keeping system parameters flexible. Application of the proposed wake-up scheme to any other room shape is straight forward.

B. Path Loss Model

Assuming a transmit pulse of uniform energy spectral density, a transmitter-receiver separation d, and lower and upper

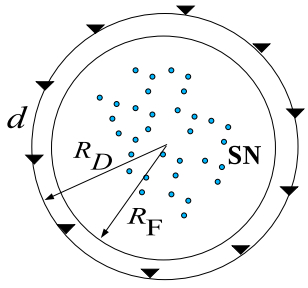

Fig. 1. Investigated scenario

cut-off frequency f_l and f_u, respectively, the linear UWB-IR path loss factor is modeled as

$$\Psi_d = \left(Ad^{-\gamma}\right)^{-1} = \left(\frac{1}{B}\int_{f_\mathrm{l}}^{f_\mathrm{u}} \frac{c^2}{(4\pi f)^2 d^\gamma} df\right)^{-1}, \qquad (1)$$

where B is the pulse bandwidth, c the speed of light and γ the path loss exponent. This model is only valid in the far-field region of a transmit antenna [3]. Hence, a minimal separation d_f between sensor nodes and transmit antennas is respected. Assuming a $\lambda/2$-dipole, this minimal distance equals $d_\mathrm{f} = \lambda_\mathrm{max} = c/f_\mathrm{min} \approx 0.1\,\mathrm{m}$, with $f_\mathrm{min} = 3.1\,\mathrm{GHz}$, the minimal allowed UWB frequency with respect to the *Federal Communications Commission* (FCC) [4]. According to (1), the path loss factor is often split into a frequency dependent part A and a distance dependent part $d^{-\gamma}$.

C. Channel Model

The *channel impulse response* (CIR) between antenna a and sensor position j is modeled according to:

$$h_{a,j}(t) = \sqrt{\frac{1}{\Psi_{a,j}}}\, h\left(t - \tau_{a,j}\right), \qquad (2)$$

with the corresponding linear path loss factor $\Psi_{a,j}$ and propagation delay $\tau_{a,j}$. The waveform $h\left(t\right)$ is normalized such that for any continuous waveform $s(t)$, the peak amplitudes of $s(t) * h(t)$ and $s(t)$ are equal, with '$*$' the linear convolution. Furthermore, $h\left(t\right)$ contains no frequency dependent path loss. The CIRs between backbone antennas and sensors all have a dominant LOS component and weak multi-path components. Hence, for investigation of the system feasibility, CIRs are modeled by dirac pulses scaled according to the path loss, i.e., $h(t) = \delta(t)$. This makes analysis trackable, whereas it allows good approximative feasibility estimation for LOS scenarios. The results are then confirmed by an exact performance analysis and simulation, where $h(t)$ equals a multi-path CIR measured in a typical industrial environment [5].

D. Backbone System

The backbone devices are statically placed around the area, have global location information and are synchronized to each other, i.e., they are modeled as a single multi-antenna device. To trigger a specific sensor node, the backbone introduces delays at each antenna such that the pulses from the N_a antennas add up coherently at a desired sensor location. Due to the existence of accurate UWB-IR localization algorithms [6], [7], beamforming accuracy of the backbone system is not a critical issue in this work. From each antenna the backbone radiates at maximally allowed pulse energy E_p, e.g., with respect to FCC. The transmit signal beamed to sensor i is described by:

$$s(t,i) \;=\; \sqrt{E_\mathrm{p}} \sum_{a=0}^{N_\mathrm{a}-1} w(t - \delta_{a,i}), \qquad (3)$$

with $w(t)$ the energy normalized transmit pulse of bandwidth B, and $\delta_{a,i}$ the delay introduced at antenna a.

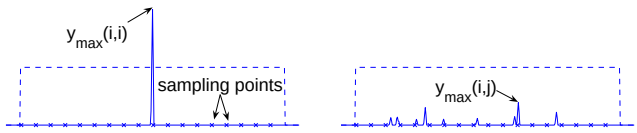

Fig. 2. Observation window at beamed (left) and not beamed (right) position

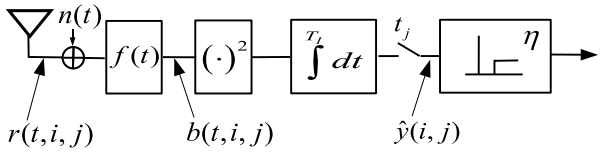

Fig. 3. Signal model of the wake-up detector

E. Wake-up Detector

Due to complexity reasons, the wake-up detector is designed as a non-coherent detector applying a fixed energy threshold, equal among all sensor nodes, and it has no *channel state information* (CSI) or any position awareness. It periodically scans the environment by sampling a certain observation window. This window, which is much larger than the receive pulse width, is coarsely synchronized to the backbone. Hence, during each observation window a wake-up procedure takes place, but the detector does not know when. Such a synchronization can be achieved by a beacon synchronization as in 802.11, whereby the wake-up detector sparsely synchronizes to a beacon signal. In Fig. 2, a schematic description of an observation window at beamed (left) and not beamed (right) position is shown. Each sensor node samples several times during the observation window, indicated by the crosses.

The signal model of the wake-up detector is shown in Fig. 3. First, the receive signal passes an amplifier and a bandpass filter and is then squared and integrated over T_I. The integrator output is sampled at time instances $\bar{t}_j = [t_{0,j}, t_{1,j}, \ldots, t_{N_\mathrm{s}-1,j}]$. The sensor node enters active mode, if one of the samples in the vector $\bar{\hat{y}}(i,j) = [\hat{y}_0(i,j), \hat{y}_1(i,j), \ldots, \hat{y}_{N_\mathrm{s}-1}(i,j)]$ exceeds the threshold η.

The wake-up performance is dominated by the noisy sample $\hat{y}_\mathrm{max}(i,j)$, which is the sample with the largest signal component $y_\mathrm{max}(i,j)$ within the observation window at position j, when steering is done to position i. Although the exact detector performance depends on $\bar{\hat{y}}(i,j)$, the system performance can be approximated by expressions depending on $\hat{y}_\mathrm{max}(i,j)$, only. Hence, due to complexity reasons, the conditions for basic feasibility are only based on $\hat{y}_\mathrm{max}(i,j)$, and are then confirmed by exact analysis and simulations based on $\bar{\hat{y}}(i,j)$.

The signal received at sensor j, when the backbone system steers to sensor position i, is given by:

$$r(t,i,j) \;=\; \sqrt{E_\mathrm{p}} \sum_{a=0}^{N_\mathrm{a}-1} h_{a,j}(t) * w(t - \delta_{a,i}) \qquad (4)$$

$$\;=\; \sqrt{\frac{E_\mathrm{p}}{\Psi_{a,j}}} \sum_{a=0}^{N_\mathrm{a}-1} h_w(t - \tau_{a,j} - \delta_{a,i}) \qquad (5)$$

with $h_w = w(t) * h(t)$. The signal $r(t,i,i)$ equals the received signal at a beamed position.

Neglecting any noise contributions, i.e. $n(t) = 0$, and assuming $f(t)$ as an ideal bandpass filter of bandwidth equal to the signal component, the integrator output vector equals

$$\bar{y}(i,j) = \frac{E_\mathrm{p}}{\Psi_{a,j}} \int_{\bar{t}_j}^{\bar{t}_j+T_\mathrm{I}} \left| \sum_{a=0}^{N_\mathrm{a}-1} h_w(t-\tau_{a,j}-\delta_{a,i}) \right|^2 dt, \quad (6)$$

with T_I the integration duration, which is set to pulse width, i.e., $T_\mathrm{I} = 1/B$. Correlation between detector output samples is avoided by choosing the sampling rate of the detector below B.

III. Analysis

A. System Feasibility

To establish basic conditions for the feasibility of the proposed scheme only the samples $y_{\max}(i,j)$ are considered and the CIR is models as $h(t) = \delta(t)$. Due to the fixed threshold constraint at sensor side, a threshold that would allow for perfect wake-up behavior over the whole disc, neglecting noise contributions, would satisfy the following two conditions:

1: The threshold is equal or smaller than the minimal beamed energy sample, i.e.:

$$\eta \leq \eta_{\max} = \min_{\forall i} \; y_{\max}(i,i). \quad (7)$$

2: The threshold is larger than the maximal non-beamed energy sample:

$$\eta > \eta_{\min} = \max_{\forall i} \left\{ \max_{\forall j \neq i} \; y_{\max}(i,j) \right\}. \quad (8)$$

In principle, there is one type of non-feasible area arising from each of the two conditions. Infeasible areas arising from Condition 1, occur at positions, at which total receive energy due to path loss is small, i.e., remote from any antenna. The backbone will never be able to trigger sensor nodes in these regions. Infeasible areas arising from Condition 2 occur at positions, where energy from one antenna is dominating, i.e., in close vicinity of an antenna. Sensor nodes located within such regions always enter active mode erroneously. While both types of infeasible regions scale with the number of antennas N_a and bandwidth B, there is a clear trade-off between the two. Hence, the proposed system is designed to avoid infeasible areas arising from Condition 1 by always transmitting at maximally allowed energy and setting the threshold η equal to or smaller than the maximal feasible threshold $\eta_{\max}$.

For the considered scenario, it can be shown by means of simple geometry that for path loss exponent $\gamma \geq 2$ and $N_\mathrm{a} \geq 5$, $\eta_{\max}$ appears at the disc center. For $\gamma \geq 2$ and $N_\mathrm{a} \leq 4$, the minimum appears not at disc center, but the energy received at disc center is close to $\eta_{\max}$. Hence, $\eta_{\max}$ can be expressed as

$$\eta_{\max} \quad = \quad N_\mathrm{a}^2 E_\mathrm{p} A R_\mathrm{D}^{-\gamma}, \quad (9)$$

with the frequency dependent part of the path loss A according to (1) and R_D the disc radius.

We define the *infeasible region* $\mathcal{U}$ as the region in which the received pulse energy from a single antenna exceeds $\eta_{\max}$ and the *feasible region* $\mathcal{F}$ as the complementary of $\mathcal{U}$. Furthermore, we define the *feasible radius* R_F as the radius of the largest disc around the center which does not contain $\mathcal{U}$. While sensor nodes in $\mathcal{U}$ will always activate in the noiseless case, a sensor node in $\mathcal{F}$ can still be triggered erroneously. First, it depends also on pulse bandwidth and sensor density, if neighbored nodes are triggered erroneously. Secondly, our definition of feasibility ignores unwanted constructive pulse superpositions. But antenna dominance in regions close to an antenna makes overall regions unfeasible, while constructive pulse interference occurs only on a few lines or even points for higher order superpositions. Hence, $\mathcal{F}$ and $\mathcal{U}$ are simple and meaningful measures with respect to system feasibility.

As single pulse energy is monotonically decreasing with increasing separation between sensor location and antenna, it follows that $\mathcal{U}$ can be approximated by N_a semi-discs around the backbone antennas. The radius R_C of the semi-discs is determined by the distance between a specific antenna a and the point on the connecting line between antenna a and the disc center, at which single pulse energy from antenna a equals $\eta_{\max}$. Equating single pulse energy and $\eta_{\max}$:

$$E_\mathrm{p} A R_\mathrm{C}^{-\gamma} \quad = \quad N_\mathrm{a}^2 E_\mathrm{p} A R_\mathrm{D}^{-\gamma}, \quad (10)$$

leads to:

$$R_\mathrm{C} \quad = \quad N_\mathrm{a}^{-2/\gamma} R_\mathrm{D} \quad \text{for} \quad R_\mathrm{C} > 0.1\,\mathrm{m}. \quad (11)$$

The total infeasible and feasible regions, $\mathcal{U}$ and $\mathcal{F}$, are:

$$\mathcal{U} \quad = \quad \frac{1}{2} N_\mathrm{a} \pi \left(N_\mathrm{a}^{-2/\gamma} R_\mathrm{D} \right)^2 \quad (12)$$

$$\mathcal{F} \quad = \quad \pi R_\mathrm{D}^2 - \mathcal{U}. \quad (13)$$

The *feasibility coverage* ($\mathrm{Cov_f}$) and the *feasibility outage* ($\mathrm{Out_f}$) express the feasible and non-feasible fractions of the disc:

$$\mathrm{Out_f} \quad = \quad \frac{\mathcal{U}}{\pi R_\mathrm{D}^2} = \frac{1}{2} N_\mathrm{a}^{\frac{\gamma-4}{\gamma}} \quad (14)$$

$$\mathrm{Cov_f} \quad = \quad 1 - \frac{1}{2} N_\mathrm{a}^{\frac{\gamma-4}{\gamma}}. \quad (15)$$

The feasible radius R_F is evaluated according to $R_\mathrm{F} = R_\mathrm{D} - R_\mathrm{C}$. Note that the pulse bandwidth hidden in E_p and A cancels out in (10), and does not appear in $\mathcal{U}$, $\mathcal{F}$, and the following equations. In Fig. 4, feasibility coverage is plotted as a function of N_a.

Significant coverage improvement is experienced by increasing N_a. E.g., for $\gamma = 2$, feasibility coverage increases by more than 10%, if the number of backbone antennas is changed from $N_\mathrm{a} = 4$ to $N_\mathrm{a} = 10$ and for $\gamma = 3$, the increase in coverage from $N_\mathrm{a} = 10$ to $N_\mathrm{a} = 100$ is larger than 20%.

In Fig. 5, feasible and infeasible regions according to analysis are plotted for $N_\mathrm{a} = 4$ (left) and $N_\mathrm{a} = 10$ (right). It is apparent that with the presented simple threshold approach

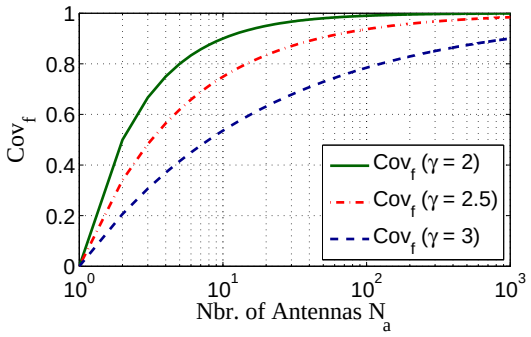

Fig. 4. Feasibility coverage as a function of N_a for different path loss exponents γ

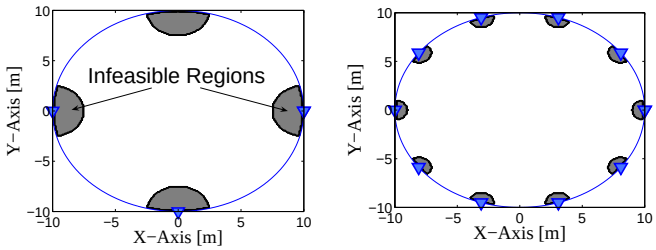

Fig. 5. Feasible coverage and outage regions for $\gamma = 2$, and $N_\mathrm{a} = 4$ (left) and $N_\mathrm{a} = 10$ (right)

reasonable feasibility coverage is achieved. By designing a sensor network application such that a minimal distance between antennas and sensor nodes is guaranteed, the system works fine. For example, if $N_\mathrm{a} = 10$ backbone antennas are applied in a room of radius $R_\mathrm{D} = 10\,\mathrm{m}$, a minimal separation of $R_\mathrm{C,min} = 1\,\mathrm{m}$ has to be guaranteed to design a working system. In a three dimensional realistic hall, where antennas are mounted below the roof, this seems reasonable.

B. Probabilities of False Alarm and Missed Detection Within The Feasible Regions

After the analysis of the feasibility, system performance is investigated considering multi-path CIRs and thermal noise at the wake-up detector. The exact *probabilities of false alarm* p_FA and *missed detection* p_MD depending on all integrator samples within the observation window are presented and compared to approximations $\tilde{p}_\mathrm{FA}$ and $\tilde{p}_\mathrm{MD}$, which are based only on the sample $\hat{y}_\mathrm{max}(i,j)$. The approximations are interesting as they are very accurate at high SNR and strongly simplify performance evaluation, especially computational efforts.

The probabilities of false alarm and missed detection given a certain room size, number of backbone antennas, and threshold, are described by:

$$p_\mathrm{FA} = \sum_{\forall i} \sum_{\forall j \neq i} p_{\mathrm{FA}|i,j}\ P(i,j) \tag{16}$$

and

$$p_\mathrm{MD} = \sum_{\forall i} p_{\mathrm{MD}|i,i}\ P(i,i), \tag{17}$$

where $P(i,j) = \frac{1}{N_\mathrm{p}(N_\mathrm{p}-1)}$, $P(i,i) = \frac{1}{N_\mathrm{p}}$, and N_p denotes the total number of sensor positions considered.

The conditional probabilities $p_{\mathrm{FA}|i,j}$ and $p_{\mathrm{MD}|i,i}$ again can be expressed as:

$$p_{\mathrm{FA}|i,j} = 1 - \prod_{k=0}^{N_\mathrm{s}-1} P\left(\hat{y}_k \leq \eta | i,j\right) \tag{18}$$

$$p_{\mathrm{MD}|i,i} = \prod_{k=0}^{N_\mathrm{s}-1} P\left(\hat{y}_k \leq \eta | i,i\right), \tag{19}$$

where N_s denotes the number of observation samples. The approximative expressions are achieved according to:

$$\tilde{p}_{\mathrm{FA}|i,j} = P\left(\hat{y}_\mathrm{max} > \eta | i,j\right) \tag{20}$$

$$\tilde{p}_{\mathrm{MD}|i,i} = P\left(\hat{y}_\mathrm{max} \leq \eta | i,i\right). \tag{21}$$

The approximations omit the temporal dimension of the problem, and therefore, strongly decrease simulation efforts.

Due to the property that the integration duration equals the pulse width, i.e., $T_\mathrm{I} = 1/B$, the scheme in Fig. 3 can be modeled as a non-coherent one tap receiver sampling N_s times within the observation window. Hence, the receive signal corresponding to the k-th sample at the j-th sensor, when steering is done to position i, can be modeled as:

$$r_k(i,j) = \sqrt{y_k(i,j)}, \tag{22}$$

whereby $y_k(i,j)$ represents $\hat{y}_k(i,j)$ in the noiseless case. The signal $b_k(i,j)$ after the bandpass filter equals:

$$b_k(i,j) = \sqrt{y_k(i,j)} + \tilde{n}_k, \tag{23}$$

with $\tilde{n}_k$ a zero-mean complex Gaussian random variable of variance $\sigma^2 = 2N_\mathrm{E}$. The conditional probability that the received energy on the k-th sample is below the threshold can therefore be described by:

$$P\left(\hat{y}_k \leq \eta | i,j\right) = P\left(|b_k|^2 \leq \eta | i,j\right). \tag{24}$$

Substituting $Z_k = |b_k(i,j)|^2$ leads to a non-central chi-square random variable with two degrees of freedom [2], [8]. Hence, the *cumulative distribution function* (CDF) of Z_k can be expressed in terms of the first order generalized Marcum's Q-function [8]:

$$F_{Z_k}(z_k) = 1 - Q_1\left(\frac{s_k}{\sigma_n}, \frac{\sqrt{z_k}}{\sigma_n}\right), \tag{25}$$

with $s_k = \sqrt{\hat{y}_k(i,j)}$, and $\sigma_n^2 = \sigma^2/2$. This yields the following result on the conditional probability:

$$P\left(\hat{y}_k \leq \eta | i,j\right) = 1 - Q_1\left(\sqrt{y_k(i,j)/N_\mathrm{E}}, \sqrt{\eta/N_\mathrm{E}}\right). \tag{26}$$

IV. Simulation Results

For the simulations, we define the *signal-to-noise ratio* (SNR) without path loss:

$$\zeta = \frac{E_p}{N_\mathrm{E}}, \tag{27}$$

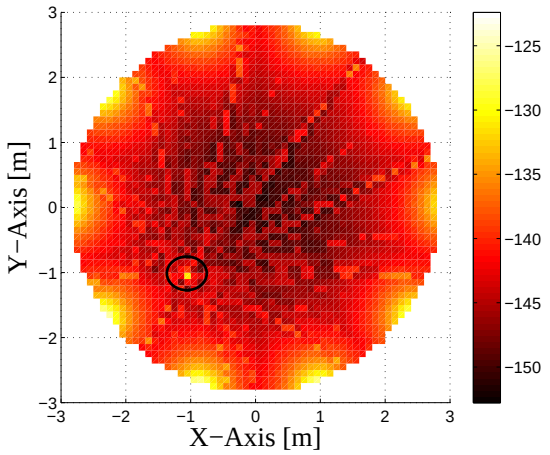

Fig. 6. Beam pattern $y_{\max}(i,j)$ [dBJ] over disc, if beamforming is done to position $(x_0, y_0) = (-1, -1)$ m; for $N_\mathrm{a} = 10$, $B = 3$ GHz, and $\gamma = 2$.

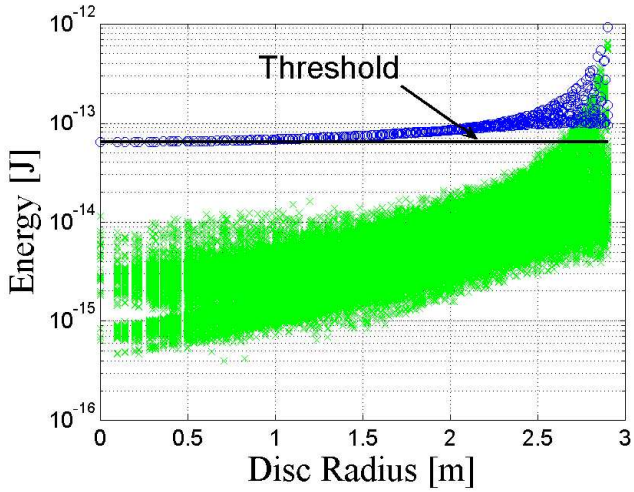

Fig. 7. All beamed samples, i.e., $y_{\max}(i,i)$, $\forall i$ ($\circ$) and all non-beamed samples, i.e., $y_{\max}(i,j)$, $\forall i$ and $\forall j \backslash i$ ($\times$) plotted over disc radius; for $N_\mathrm{a} = 10$, $B = 3$ GHz, and $\gamma = 2$.

where N_E denotes the power spectral density of an equivalent noise. The threshold η is described as a fraction of the maximal receive energy at disc center:

$$\eta = \tilde{\eta}\eta_{\max} = \tilde{\eta} N_\mathrm{a}^2 E_\mathrm{p} / \Psi_{\mathrm{R_D}}, \tag{28}$$

where $\tilde{\eta}$ is the fractional threshold. Hence, (26) results in

$$P\left(\hat{y}_k \leq \eta | i,j\right) = 1 - Q_1\left(\sqrt{\zeta m_k(i,j)}, \sqrt{\tilde{\eta} N_\mathrm{a}^2 / \Psi_{\mathrm{R_D}} \zeta}\right), \tag{29}$$

where we used the abbreviation $m_k(i,j) = \frac{y_k(i,j)}{E_\mathrm{p}}$. There are two major reasons to define the SNR as the ratio between transmit pulse energy from a single antenna over equivalent noise N_E at sensor node. First, normalization to receive $\mathrm{SNR_{Rx}}$ would cancel out performance gains due to an increased receive power. Hence, significant gains due to the increased number of antennas (devices) would be neglected. Secondly, $\mathrm{SNR_{Rx}}$ varies over the disc, while the considered SNR is a global measure.

The proposed LDR wake-up scheme operates in the peak power limited regime, where maximally allowed single pulse spectral energy equals $E_0 = 8.1 \cdot 10^{-20} \frac{\mathrm{W}}{\mathrm{Hz}^2}$ [9]. Therefore, we set single pulse energy to $E_\mathrm{p} = E_0 B$. The equivalent noise is defined as $N_\mathrm{E} = N_0 G_\mathrm{Amp} L_\mathrm{Ant} L_\mathrm{Imp}$, with the noise figure G_Amp, the antenna mismatch L_Ant, the implementation loss L_Imp, and $N_0 = -174 \frac{\mathrm{dBm}}{\mathrm{Hz}}$, the power spectral density of the thermal noise. Further simulation parameters are the number of antennas $N_\mathrm{a} = 10$, the path loss exponent $\gamma = 2$, chosen according to [10], and the pulse frequency band from $f_\mathrm{l} = 3.1$ GHz to $f_\mathrm{u} = 6.1$ GHz. The sensor nodes are placed on a two-dimensional cartesian grid of spacing d_s, whereby d_s is always chosen larger than or equal to the minimal resolvable sensor separation $d_\mathrm{min} \approx c/B = 10\,\mathrm{cm}$.

For $h(t) = \delta(t)$, a beam pattern example over the whole disc is plotted in Fig. 6, for steering position $(x_0, y_0) = (-1, -1)$ m, i.e., $y_{\max}(i,j)$, $\forall j$ are plotted for a specific i. The plot is scaled in dBJ. The disc radius equals 3 m, spatial sampling was done on a grid of 10 cm. The

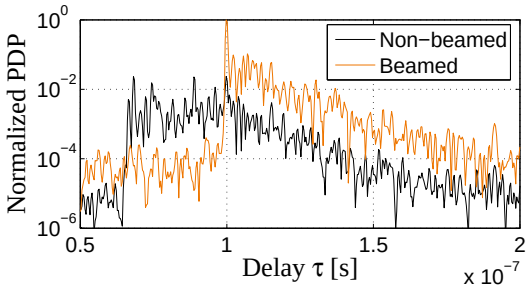

Fig. 8. Instantaneous PDP example of a beamed and a non-beamed receive signal

antenna positions can be identified at the edge of the disc. The width of the beamed pulse approximately concentrates on one spatial sample. In Fig. 7, all maximal beamed samples, i.e., $y_{\max}(i,i)$, $\forall i$ as '$\circ$' points and all maximal non-beamed samples, i.e., $y_{\max}(i,j)$ $\forall i$ and $\forall j \backslash i$ as '$\times$' points, are plotted over the disc radius. The plot can be considered as the collection of $y_{\max}(i,j)$ over all possible steering positions i and all polar coordinates ϕ from 0 to 2π. The maximal feasible threshold $\eta_{\max}$ is indicated, too. Within the feasible region, i.e., up to a radius of 2.7 m, significant energy differences between beamed and non-beamed samples can be identified promising good performance results.

In the following all results are based on measured UWB-IR multi-path CIRs [5]. In Fig. 8, instantaneous *power delay profile* (PDP) examples of a beamed and a non-beamed received baseband signal is shown as used in the simulations of p_FA and p_MD. For reasonable comparison, both PDPs are normalized to the peak of the beamformed PDP. Although significant multi-paths are observable up to about 100 ns after the LOS component, it is apparent that the beamformed LOS component is almost 20 dB stronger than all other component. This highlights the interesting property that CIRs from different antennas arriving with different propagation delays at a certain receiver are almost orthogonal to each other and add up linearly in energy, only, while the beamformed

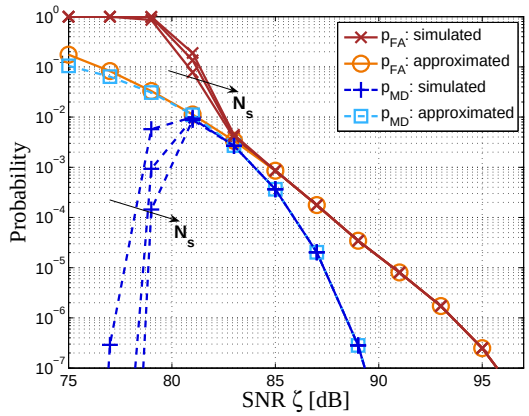

Fig. 9. Probabilities p_{FA} and p_{MD} for $R_{\mathrm{D}} = 100\,\mathrm{m}$, $N_{\mathrm{a}} = 10$, $B = 3\,\mathrm{GHz}$, $\gamma = 2$, $\tilde{\eta} = 0.5$, and differen N_s.

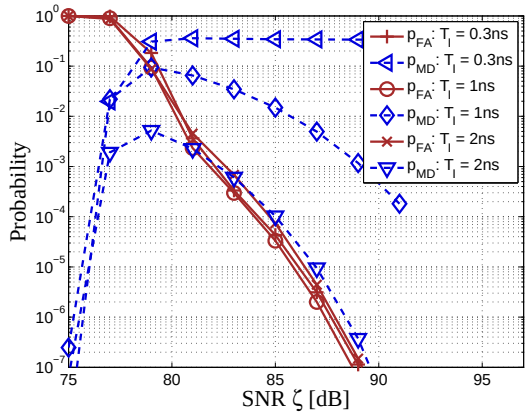

Fig. 10. Probabilities p_{FA} and p_{MD} for $R_{\mathrm{D}} = 100\,\mathrm{m}$, $N_{\mathrm{a}} = 10$, $\gamma = 2$, $\tilde{\eta} = 0.7$, and different bandwidth $B = 1/T_{\mathrm{I}}$, if jitter of 1 ns is present

LOS components add up linearly in amplitude. With this observation, good wake-up performance in realistic multi-path scenarios can be expected, with some adjustments, even in NLOS scenarios.

In Fig. 9, simulated probabilities of false alarm and missed detection are shown for a fractional threshold $\tilde{\eta} = 0.5$, a disc radius $R_{\mathrm{D}} = 100\,\mathrm{m}$, and different numbers of observation samples $N_{\mathrm{s}} \in \{600, 1200, 1800\}$. Only sensor positions within the feasible radius R_{F}, now evaluated according to the threshold $\eta = \tilde{\eta}\eta_{\max} \leq \eta_{\max}$, are considered. The approximations according to (20) and (21) are plotted as well. The probability of missed detection p_{MD} is low not only at high SNR but also at low SNR. This is due to the square low wake-up detector, which is sensitive to energy only, i.e., any noise contribution increases the probability of false alarm and decrease the probability of missed detection.

It is apparent that presented approximations are very loose for low SNR. But at the same time, they are very accurate at high SNR, where the performance is more interesting, too. From a simple link budget [2], it follows that $\mathrm{SNR} = 85\,\mathrm{dB}$ is a reasonable value even for UWB and hence, presented performance curves are promising. An interesting observation arises from the simulation curves for increasing number of observation samples N_{s}, according to (6). They are all very similar, especially at high SNR, which shows that the impact of the observation window is minor, at least for moderate window size. The strong improvement of p_{FA} between 79 and 84 dB occurs because the probability of false alarm on many observation samples becomes irrelevant at the same time. This is also the reason why presented bounds become more accurate at high SNR.

In Fig. 10, p_{MD} and p_{FA} are shown for different system bandwidths and integration durations $T_{\mathrm{I}} = 1/B$, if a uniformly distributed sampling jitter of 1 ns is introduced. As could be expected p_{FA} is hardly affected by the jitter, while the impact on the probability of missed detection p_{MD} is severe at an integration duration $T_{\mathrm{I}} = 1/(3\,\mathrm{GHz})$. However, if system bandwidth is decreased and hence, integration duration of the detector increased, the system becomes robust again. This is at the expense of increased minimal resolvable sensor separation.

V. Conclusions

A new, very simple UWB wake-up detection scheme for LOS scenarios is proposed. It significantly reduces power consumption at sensor side at the expense of increased complexity and power consumption at the backbone. The non-coherent wake-up detector requires neither CSI nor any location information. Conditions for basic feasibility are presented and investigated as a function of the number of backbone devices. Promising performance results based on analysis and simulation over measured CIRs are presented. Due to the "quasi" orthogonality between different UWB-IR CIRs, the scheme works well also in strong multi-path scenarios. Furthermore, it is demonstrated that the wake-up scheme can be designed robust with respect to sampling jitter, at the expense of increased minimal resolvable sensor separation.

References

[1] I. Oppermann, L. Stoica, A. Rabbachin, Z. Shelby, and J. Haapola, "UWB wireless sensor networks: UWEN - A practical example," *IEEE Commun. Mag.*, vol. 42, no. 12, pp. 27–32, Dec. 2004.

[2] F. Troesch, F. Althaus, and A. Wittneben, "A simple wake-up scheme based on ultra-wideband beamforming," in *IEEE Int. Workshop on Smart Antennas*, Ulm, Germany, March 13–14, 2006, to appear.

[3] T. S. Rappaport, *Wireless Communications – Principles and Practice*, 2nd ed. Prentice Hall, 2002.

[4] FCC, "Revision of part 15 of the commission's rules regarding ultra-wideband transmission systems," *First Report and Order, ET-Docket 98-153, FCC 02-28*, adopted/released Sept. 19, 2005/Apr. 22, 2002.

[5] F. Althaus, F. Troesch, and A. Wittneben, "UWB geo-regioning in rich multipath environment," in *IEEE Veh. Tech. Conf.*, Dallas, Tx, USA, 2005.

[6] B. Q. Ruiz, A. A. Vazquez, M. L. Rubio, and G. J. Garcia, "Impulse radio UWB system architecture for smart wireless sensor networks," in *Int. Workshop on Netw. with UWB and Workshop on UWB Sensor Netw. (NEUWB)*, July, 4–6, 2005, pp. 35–39.

[7] K. Yu and I. Oppermann, "UWB positioning for wireless embedded networks," in *IEEE Conf. Rad. and Wirel. (RAWCON)*, Atlanta, GA, Sept. 19–22, 2004, pp. 459–462.

[8] J. G. Proakis, *Digital Communications*, 1st ed. John Wiley & Sons, 2002.

[9] F. Troesch, F. Althaus, and A. Wittneben, "Pulse position pre-coding exploiting UWB power constraints," in *IEEE Proc. SPAWC*, New York, NY, Jun. 5–8, 2005.

[10] J. Kunisch and J. Pamp, "UWB radio channel measurements for sensor networks in industrial environments," in *IEEE Int. Conf. on Electromagnetics in Adv. App. (ICEAA 05)*, Torino, Italy, Sept. 12–16, 2005.